# Elemental nitrogen partitioning in dense interstellar clouds

Julien Daranlot[a,b], Ugo Hincelin[c,d], Astrid Bergeat[a,b], Michel Costes[a,b], Jean-Christophe Loison[a,b], Valentine Wakelam[c,d], and Kevin M. Hickson[a,b,1]

[a]Université de Bordeaux, Institut des Sciences Moléculaires, Unité Mixte de Recherche 5255, F-33400 Talence, France; [b]Centre National de la Recherche Scientifique, Institut des Sciences Moléculaires, Unité Mixte de Recherche 5255, F-33400 Talence, France; [c]Université de Bordeaux, Laboratoire d'Astrophysique de Bordeaux, Unité Mixte de Recherche 5804, F-33270 Floirac, France; and [d]Centre National de la Recherche Scientifique, Laboratoire d'Astrophysique de Bordeaux, Unité Mixte de Recherche 5804, F-33270 Floirac, France

Edited by Neta A. Bahcall, Princeton University, Princeton, NJ, and approved May 16, 2012 (received for review January 2, 2012)

**Many chemical models of dense interstellar clouds predict that the majority of gas-phase elemental nitrogen should be present as $N_2$, with an abundance approximately five orders of magnitude less than that of hydrogen. As a homonuclear diatomic molecule, $N_2$ is difficult to detect spectroscopically through infrared or millimeter-wavelength transitions. Therefore, its abundance is often inferred indirectly through its reaction product $N_2H^+$. Two main formation mechanisms, each involving two radical-radical reactions, are the source of $N_2$ in such environments. Here we report measurements of the low temperature rate constants for one of these processes, the N + CN reaction, down to 56 K. The measured rate constants for this reaction, and those recently determined for two other reactions implicated in $N_2$ formation, are tested using a gas-grain model employing a critically evaluated chemical network. We show that the amount of interstellar nitrogen present as $N_2$ depends on the competition between its gas-phase formation and the depletion of atomic nitrogen onto grains. As the reactions controlling $N_2$ formation are inefficient, we argue that $N_2$ does not represent the main reservoir species for interstellar nitrogen. Instead, elevated abundances of more labile forms of nitrogen such as $NH_3$ should be present on interstellar ices, promoting the eventual formation of nitrogen-bearing organic molecules.**

astrochemistry | chemical kinetics

Elemental nitrogen is present in the atmospheres of telluric planets predominantly in the form of $N_2$. As a stable molecule with a high bond energy, it is hard to break N out of $N_2$, so the amount of nitrogen available for the formation of complex prebiotic molecules in such environments depends on the presence of nitrogen in more labile forms such as $NH_3$. Despite the high abundance of $N_2$ in the solar system, observations of $N_2$ beyond our own planetary system are scarce, as $N_2$ possesses no allowed rotational or vibrational transitions. Only one direct measurement (1) of $N_2$ in the far ultraviolet wavelength range (thereby accessing its electronic transitions) has been reported in a diffuse interstellar cloud, where low column densities allow light to pass and a star along the line of sight was used to probe the species within. In dense molecular clouds where temperatures as low as 10 K prevail, UV starlight is absorbed long before it can penetrate to the cloud core where $N_2$ is predicted to form efficiently (2, 3). Instead, gas-phase $N_2$ densities are inferred through observations of $N_2H^+$, a product of the $N_2 + H_3^+$ reaction (4–6). The major pathways for $N_2$ formation in dense clouds rely on reactions involving neutral radical species:

$$N + OH \rightarrow NO + H \quad [1]$$

$$N + NO \rightarrow N_2 + O \quad [2]$$

Mechanism (I)

$$N + CH \rightarrow CN + H \quad [3]$$

$$N + CN \rightarrow C + N_2 \quad [4]$$

Mechanism (II)

Recent experimental and theoretical studies of reactions **1** (7) and **2** (8–10) indicate that these reactions are slower than previously thought, suggesting that current astrochemical models overestimate molecular nitrogen abundances produced by Mechanism (I) both at steady state and at specific times. The influence of Mechanism (II) on interstellar $N_2$ abundances is currently unknown, given that neither reaction **3** nor reaction **4** has been studied at temperatures lower than 200 K. Nevertheless, both of these reactions are estimated to react rapidly, even at 10 K.

Unfortunately, the measurement of rate constants for reactions at temperatures below 100 K is a task that is far from trivial. Cryogenic cooling methods can be used to attain such temperatures; however, these techniques are hampered by the condensation of reactants and precursor molecules onto the reactor walls. As a result, the range of reactions that can be studied is restricted to those between species with substantial vapor pressures at low temperature. During the early 1990s, the CRESU technique (Cinetique de Reaction en Ecoulement Supersonique Uniforme or reaction kinetics in a uniform supersonic flow) that had already been applied to the study of ion-molecule reactions (11) was adapted to study reactions between neutral species at low temperatures (12). This development was largely responsible for proving that reactions between neutral species play an important role in cold regions of interstellar space. The CRESU method uses Laval nozzle expansions to produce cold supersonic flows with a uniform density and temperature profile for a period of several hundreds of microseconds, allowing fast reactions to be studied. As the cold jet of gas is isolated from the reactor walls, problems with reagent condensation are avoided. So far, this technique has led to the measurement of rate constants for more than 100 radical-molecule reactions at temperatures as low as 6 K (13). In stark contrast, few low temperature investigations of reactions involving two unstable species have been reported (7, 14). These reactions are particularly challenging for experimentalists, requiring the production of one of the radicals in excess (for the pseudo-first-order kinetic analysis to be valid) and the measurement of its concentration for absolute rate constants to be extracted. As a result, current models rely heavily on calculations, extrapolations, or estimates to predict their rates. The recent development of the discharge-flow CRESU technique (8) and its application to the study of unstable radical reactions

Author contributions: A.B., V.W., and K.M.H. designed research; J.D., U.H., A.B., M.C., J.-C.L., V.W., and K.M.H. performed research; J.D., U.H., V.W., and K.M.H. analyzed data; and V.W. and K.M.H. wrote the paper.

The authors declare no conflict of interest.

This article is a PNAS Direct Submission.

[1]To whom correspondence should be addressed. E-mail: km.hickson@ism.u-bordeaux1.fr.

This article contains supporting information online at www.pnas.org/lookup/suppl/doi:10.1073/pnas.1200017109/-/DCSupplemental.

through the relative rate method (7) has furnished low temperature rate constants for reactions **1** and **2** whilst demonstrating that studies of other atom–radical reactions are entirely feasible. Here we report measurements of the rate constant for reaction **4** from 296 K to 56 K using this method. The influence of the new rate constants for reactions **1**, **2**, and **4** on elemental nitrogen partitioning in dense interstellar clouds and in prestellar cores is tested for the first time using chemical models incorporating both gas-phase and grain surface chemistry. Details of both the experimental method and the model are provided in the *Materials and Methods* section, whereas the experimental and model cross-checks performed for this study are outlined in the *SI Text*.

## Results and Discussion

The measured temperature dependent rate constants for the N + CN reaction are displayed in Fig. 1 alongside earlier experimental work (15, 16) and the recommended values as proposed by the Kinetic Database for Astrochemistry (KIDA) (17). The measured rate constants are also listed in Table S1 alongside other relevant information. The first step in the measurement of such quantities relies on the application of the pseudo-first-order approximation, where one of the reagent species is held in a large excess so that its concentration remains effectively constant throughout the reaction, thereby facilitating the kinetic analysis. Under circumstances where the excess reagent is a stable molecule, it is a trivial procedure to determine its concentration from its partial pressure. A linear least squares fit to the resulting pseudo-first-order rate constants plotted as a function of the co-reagent concentration directly yields the second-order rate constant. However, for the present experiments, where the atomic nitrogen concentration [N] can no longer be determined by this method, rate constants for the N + CN reaction were measured by the relative rate method using the N + OH reaction as the reference process, both reactions occurring concurrently in the same reactor. Fig. 2 shows the temporal evolution of reactant CN and reference OH fluorescence signals recorded simultaneously in the presence of excess atomic nitrogen at 296 K and 56 K.

Under these conditions, both reactants decay exponentially to zero with a characteristic decay time, $\tau$, proportional to the product of [N], and the rate constant $k_1$ or $k_4$. As any single pair of OH and CN decays is measured with the same [N], the difference

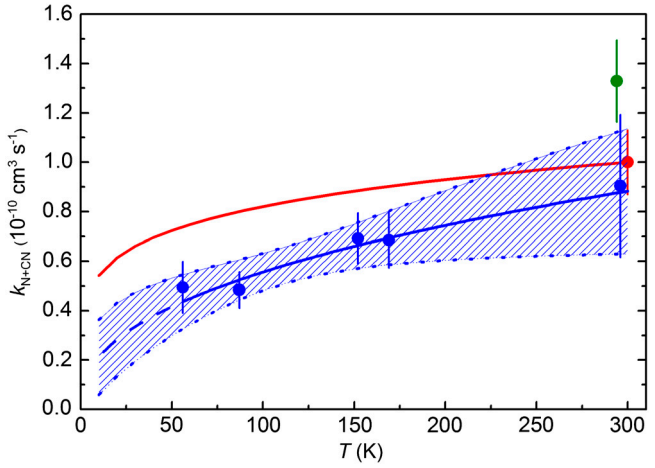


**Fig. 1.** Rate constants for the $N(^4S^0) + CN(^2\Sigma^+)$ reaction as a function of temperature. Experimental values: (solid red circle) Whyte and Phillips (15); (solid green circle) Atakan et al. (16); (solid blue circle) this work. Error bars on the current measurements represent the $1\sigma$ statistical uncertainty combined with a systematic uncertainty of 10% estimated from possible inaccuracies in the measured flow rates, pressures and temperatures. The blue line represents the fit and extrapolation to 10 K of the current data. The shaded area represents 95% confidence intervals for the rate constant fit given by a standard method of propagation of variances and covariances. Recommended values: (red line) KIDA (17).

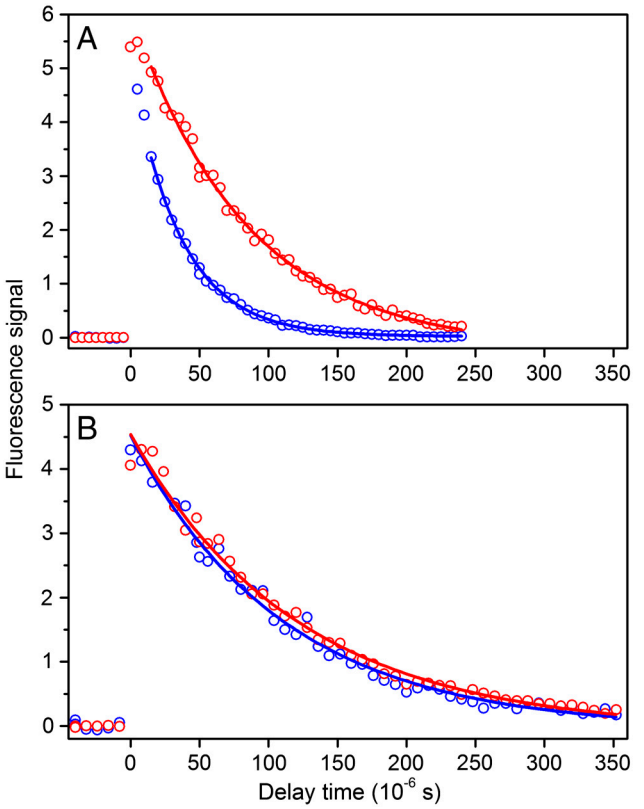


**Fig. 2.** Exemplary temporal profiles of OH and CN. (*A*) At 296 K with estimated $[N] = 2.4 \times 10^{14}$ atom cm$^{-3}$. Open blue circle: $CN(^2\Sigma^+)$ LIF signal. Open red circle: $OH(^2\Pi_{3/2})$ LIF signal. (*B*) As in (*A*) but at 56 K with estimated $[N] = 1.1 \times 10^{14}$ atom cm$^{-3}$.

in $\tau$ directly reflects the differing reactivity of the two reactions. Given that [N] was held in large excess with respect to the OH and CN radical concentrations for all experiments, simple exponential fits to the OH and CN fluorescence signals yield the pseudo-first-order rate constants $k'_1 \equiv k_1[N]$ and $k'_4 \equiv k_4[N]$. This procedure was performed at several values of [N] by varying the $N_2$ flow and/or the power of the microwave discharge. The values of $k'_4$ obtained in this way for a specified temperature were plotted as a function of the corresponding values of $k'_1$. A weighted linear least squares fit to the data yields the ratio of the two rate constants $k_4/k_1$ from the slope, an example of which is shown in Fig. 3.

The temperature dependent rate constants for reaction **4** presented in Fig. 1 were finally obtained by multiplying the ratio obtained from the slope of plots similar to the one presented in Fig. 3 by the value of the rate constant previously obtained for reaction **1** at the corresponding temperature. The rate of reaction **1** is approximately constant over the range 296 K–56 K (7) with $k_1 \approx 4.5 \times 10^{-11}$ cm$^3$ s$^{-1}$. Comparison between the pairs of decays in panels (*A*) and (*B*) of Fig. 2 then clearly demonstrates that the reactivity of reaction **4** falls as the temperature is lowered. At 296 K, $k_4 = 9 \times 10^{-11}$ cm$^3$ s$^{-1}$, in good agreement with earlier measurements (15, 16); and this value falls to $5 \times 10^{-11}$ cm$^3$ s$^{-1}$ at 56 K.

A simple $A \times (T/300)^B$ fit to the data yields a temperature dependence of $T^{(0.42\pm0.09)}$ [$A = (8.8 \pm 3.8) \times 10^{-11}$ cm$^3$ s$^{-1}$]. As the rate constant varies only weakly with temperature, extrapolation allows us to predict a value of $k_4(10\,K) = 2 \times 10^{-11}$ cm$^3$ s$^{-1}$, more than an order of magnitude smaller than the value of $3 \times 10^{-10}$ cm$^3$ s$^{-1}$ recommended by current astrochemical databases UMIST (18) and OSU 2008 [Herbst, E. Ohio State University Astrochemical Database (update

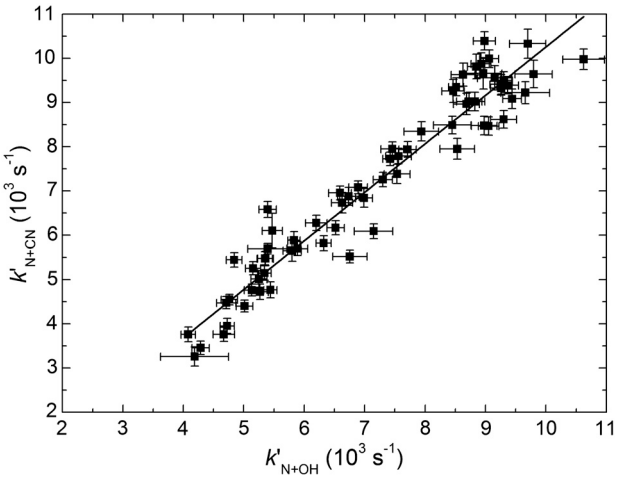


**Fig. 3.** Pseudo-first-order rate constants for reaction **4** as a function of the pseudo-first-order rate constants for reaction **1** at 56 K. A weighted linear least squares fit yields the ratio of the second-order rate constants $k_4/k_1$. The error bars on the ordinate reflect the statistical uncertainties at the level of a single standard deviation obtained by fitting to OH LIF profiles such as those shown in Fig. 2. The error bars on the abscissa were obtained in the same manner by fitting to the CN LIF profiles.

OSU_09_2008) http://www.physics.ohio-state.edu/~eric/research_files/osu_09_2008].

The recently measured and calculated rate constants for reactions **1** (7), **2** (8–10), and **4** might influence the $N_2$ abundance predicted by chemical models of dark clouds. To test their importance to $N_2$ formation, we used the chemical model Nautilus (19), which solves the kinetic equations for both gas-phase and grain surface chemistry. This model incorporates gas-phase reactions, the sticking of gas-phase species onto interstellar grains, the evaporation of surface species into the gas-phase, and chemical reactions occurring at the surface of the grains. Typical dense cloud conditions were used and species were initially present in their atomic or ionic form at their diffuse cloud abundances as given in Table S2, assuming that dense molecular clouds form from diffuse media, except for hydrogen, which was present as $H_2$. The model runs were initially performed with a depleted oxygen abundance compared to that of carbon as suggested by Jenkins (20) and Whittet (21), yielding an elemental C/O ratio of 1.2 (*SI Text*). Depleted elemental oxygen was required to reproduce the observed low gas-phase abundance of $O_2$ in dense clouds in a recent modeling study (19). However, given the probable model dependence on initial elementary abundances that are themselves poorly constrained, secondary model runs were also undertaken in which the elemental C/O ratio was fixed to 0.7 using a larger oxygen abundance of $2.4 \times 10^{-4}$ with respect to total hydrogen [$n_H = n(H) + 2n(H_2)$] to test the effect of excess elemental oxygen. The gas and dust temperature was fixed at 10 K, and a visual extinction ($A_V$) of 10, a cosmic-ray ionization rate of $1.3 \times 10^{-17}$ $s^{-1}$, and a total hydrogen density of $2 \times 10^4$ $cm^{-3}$ were used. The model follows species in the gas-phase and on interstellar grains as a function of time. The gas-phase chemical network used was updated in 2011 according to recommendations made by experts contributing to KIDA (17), and should be the most representative set of input parameters currently available for modeling purposes.

The chemical model was run using three sets of kinetic input parameters: (a) the most recently recommended rate constants by the OSU database (OSU_09_2008); (b) the KIDA recommended values; (c) the KIDA recommended values replacing rate constants for reactions **1**, **2**, and **4** with the new values of $k_1 = (2.5 \pm 1.0) \times 10^{-11}$, $k_2 = (1.0^{+1.0}_{-0.5}) \times 10^{-11}$ and $k_4 = (2.0 \pm 1.0) \times 10^{-11}$ $cm^3$ $s^{-1}$ from extrapolation of the experimental data to 10 K. The quoted errors on these rate constants were estimated from the spread of the available theoretical and experimental data. The percentage of elemental nitrogen forming $N_2$ in these models for a C/O ratio of 1.2 is shown in Fig. 4*A*. The corresponding models for a C/O ratio of 0.7 are shown in Fig. 4*C*.

Formation of $N_2$ is already less efficient for both high and low C/O ratios if we compare the results of models (a) and (b) as a result of the numerous updates of the original OSU scheme proposed by the KIDA experts. The inclusion of new rate constants for reactions **1**, **2**, and **4** in model (c) reduces $N_2$ yields even further. For model (c), at most, 40% of the initial elemental nitrogen is converted to $N_2$ (in the gas-phase and on grain surfaces) for high C/O ratios and an even smaller value of 17% is obtained for the low C/O ratio case.

Fig. 4 *B* and *D* show $N_2H^+$ fractional abundances ($/n_H$) [for high and low C/O ratios with model (c)], alongside the observational constraints on $N_2H^+$ from Taurus Molecular Cloud (TMC-1, CP Peak) of $1.5 \times 10^{-10}$ (5) and $3.5 \times 10^{-10}$ (22). The model (c) abundances of gas-phase N, $N_2$, and $NH_3$ ice are also shown.

At times of $2 \times 10^5$ and (3–5) $\times 10^5$ yr, modeled $N_2H^+$ abundances are in good agreement with the observed abundances, providing the age constraints for our high and low C/O ratio models. At these times, $N_2$ has a predicted gas-phase abundance of $(6 \pm 2) \times 10^{-6}$ ($/n_H$) for the low oxygen case and $(4 \pm 2) \times 10^{-6}$ ($/n_H$) for the high oxygen case, amounting to only $(21 \pm 6)$ % and $(12 \pm 5)$ %, respectively, of the total initial nitrogen. Errors on these gas phase $N_2$ values were obtained by performing test model runs with rate constants for reactions **1**, **2**, and **4** at the limits given by our estimated uncertainties. Instead of producing $N_2$, atomic nitrogen depletes onto interstellar grains, where $NH_3$ ice forms efficiently in both low oxygen and high oxygen models. At long times, the condensed phase abundance of $N_2$ falls ($>10^6$ yr) as a result of dissociation by cosmic rays, slowly converting it to $NH_3$.

Previous studies have suggested that $N_2$ is mostly produced by Mechanism (I) in dark clouds (5, 22).Our analysis suggests that this scheme might be only a minor source of gas-phase $N_2$ compared with Mechanism (II). This effect can be highlighted by the results of the low C/O ratio model in which we would expect the presence of excess atomic oxygen to increase the influence of Mechanism (I) by promoting OH formation through a series of ion-neutral reactions with $H_3^+$. In this case, the reactive fluxes of reactions **2** and **4** (defined as the product $k$[A][B] where [A] and [B] are the densities of reactants A and B respectively) from (2–5) $\times 10^5$ yr are similar, producing equivalent quantities of $N_2$ (Fig. S1*A*). In contrast, the reactive flux of reaction **4** is 20 times greater than the reactive flux for reaction **2** in the high C/O ratio model over the same time period, resulting in a higher overall $N_2$ yield. Clearly, the updated Mechanism (I) now produces $N_2$ inefficiently.

To rationalize the model results, we can examine the abundances of the relevant precursor species CN and NO (Fig. S1*B*). CN abundances are reduced by a factor of 10 for the low C/O case as the O + CN reaction [with a recommended rate constant (17) of $4 \times 10^{-11}$ $cm^3$ $s^{-1}$ at 10 K] becomes the major CN removal mechanism. In the absence of an efficient removal mechanism for NO (the equivalent O + NO reaction does not occur), its abundance rises by a factor of 10 without significantly increasing $N_2$ yields.

One factor that has so far been overlooked is the importance of reaction **3**. If the rate constant at 10 K is less than the currently predicted value of $2.3 \times 10^{-10}$ $cm^3$ $s^{-1}$, the $N_2$ yield of Mechanism (II) would decrease by a corresponding amount, due to the reduced reactive flux of reaction **4**. Future low temperature measurements of the rate for reaction **3** are required to resolve this issue and to provide a definitive answer as to which of the two mechanisms really dominates. In either case, the clear conclusion is that total $N_2$ production falls.

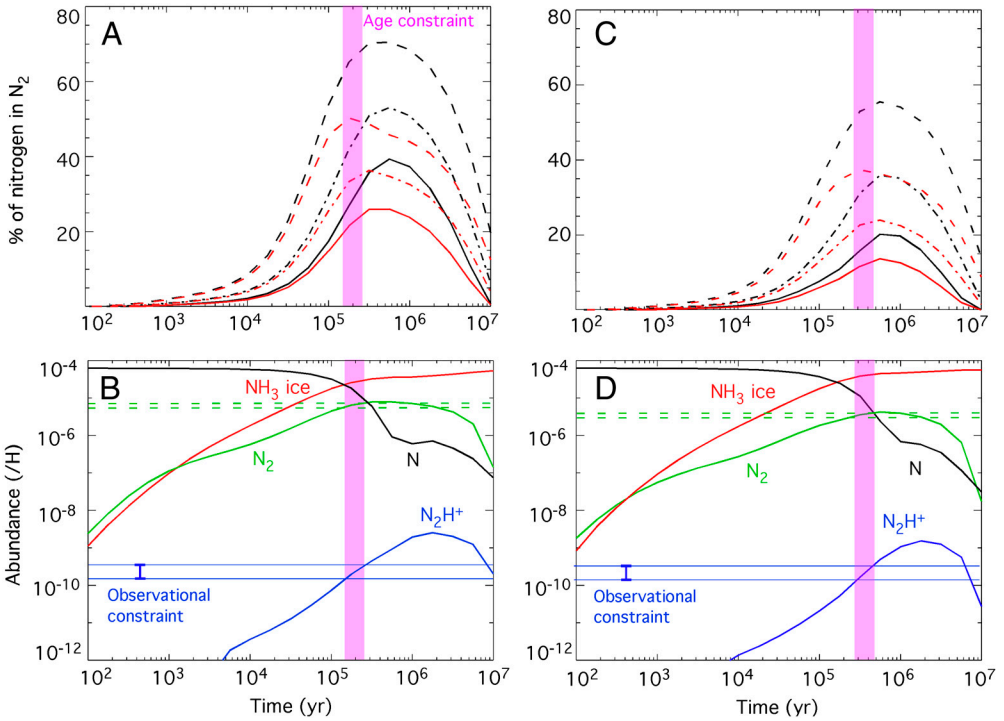


**Fig. 4.** Model results for the formation of selected nitrogen containing species in dark clouds as a function of time. (*A*) Percentage of elemental nitrogen in the form of $N_2$ (in the gas-phase and on interstellar ices). Typical dense cloud parameters are used for a density of $2 \times 10^4$ cm$^{-3}$, a solar elemental abundance of $6.2 \times 10^{-5}$ (/$n_H$) for nitrogen and a C/O ratio of 1.2, for three different networks: dashed lines, model (*a*) OSU database; dashed-dotted lines, model (*b*) KIDA values (17); solid lines, model (*c*) KIDA with updates for reactions **1**, **2**, and **4**. Red lines indicate gas-phase $N_2$, black lines indicate total (gas + ice) $N_2$. (*B*) Gas-phase abundances of N, $N_2H^+$, and $N_2$ and abundance of $NH_3$ ice (/$n_H$) predicted by model (*c*) for a C/O ratio of 1.2 together with the observational constraints on $N_2H^+$ in TMC-1 (5, 22). Horizontal dashed lines indicate the constraints on $N_2$ abundances. (*C*) As (*A*), for a C/O ratio of 0.7. (*D*) As (*B*), for a C/O ratio of 0.7.

It is interesting to test the effect of our newly determined rate constants on $N_2$ formation in other, more dense regions of interstellar space such as prestellar cores, the evolutionary stage following dense clouds but preceding protostar formation. The nitrogen chemistry of prestellar cores has been the subject of debate in recent years because models of such regions employing recommended rate constants have been unable to reproduce observed abundances of nitrogen containing species (23–25). One of the most well-known prestellar cores is Barnard 68 (B68). The density structure of B68 observationally determined by Alves et al. (26) was used to compute the abundances of the major nitrogen bearing species as a function of visual extinction Av, which can be related to the radius towards the core center. More details on the prestellar core model parameters can be found in the *Materials and Methods* section. The predicted abundances of the major nitrogen bearing species are presented in Fig. 5*A* for a time of $5 \times 10^6$ yr while the results of the time dependent model are shown in Fig. 5*B*. The predicted abundances of nitrogen bearing species as a function of Av are very similar to the earlier results of Maret et al. (6). However, the initial conditions used in our model (species in atomic form) did not need to be modified to obtain these results. Moreover, tests in which some of the initial elements were put in molecular form at the outset (notably with 50% of the available carbon in the form of CO) yielded essentially the same fractional abundances (*SI Text*). Mechanistically, the lower rate constants for our updated Mechanism (I) lead to less gas phase $N_2$ production and a correspondingly low $N_2H^+$ abundance. In contrast, Maret et al. (6) adjusted the initial fraction of elemental nitrogen present as $N_2$ (thereby allowing $N_2H^+$ formation) while blocking the time dependent formation of $N_2$ through low gas phase atomic oxygen abundances, effectively offsetting the previously high rate constants for reactions **1** and **2**. In a similar manner to our dense cloud results presented in Fig. 4, an increase in initial elemental oxygen (with C/O = 0.7) under prestellar core conditions actually results in even lower total $N_2$ yields (Fig. S2).

In the absence of efficient gas-phase removal mechanisms for atomic nitrogen in our updated model, these atoms deplete onto interstellar grains where surface reactions with atomic hydrogen are predicted to transform them to $NH_3$ ices. This result is supported by observations of dense regions which have so far failed to detect $N_2$ ices (27), while observations of gas-phase $NH_3$ originating from the sublimation of icy mantles (28) or direct observations of $NH_3$ ices in young stellar objects (YSOs) (29) indicate that as much as 20% of total elemental nitrogen could be present as condensed phase $NH_3$. Our model predicts that a larger value of 45% of the elemental nitrogen should be present as $NH_3$ ice [from model (c) results with a C/O ratio of 0.7] in TMC-1 at times when the $N_2H^+$ abundance is well reproduced. The remaining elemental nitrogen at these times is partitioned between gas-phase N, gas-phase $N_2$, and $N_2$ ices, which are themselves converted to $NH_3$ ice on longer timescales. The predicted amount of $NH_3$ ice is also substantially larger than the observed one in quiescent dark clouds (5% compared to $H_2O$ ices) (30). The only surface reaction mechanism currently considered in our model is the Langmuir-Hinshelwood mechanism, whereby two thermalized species are allowed to diffuse across the surface until they react. The inclusion of other surface processes could allow the formation of more complex N-bearing species or even maintain nitrogen in its atomic form. Indeed, the observation of non-hydrogenated surface species, such as $CO_2$ and OCS (31), does indicate that mechanisms other than the diffusive one do exist (32). The predicted $NH_3$ ice abundances are also much larger than the ones observed in comets (33). As in interstellar ices, $NH_3$ is the most abundant N-bearing species observed in comets, but it only accounts for a small fraction of the total elemental nitrogen, whose reservoir is currently unknown. Although our study cannot give a definitive answer to this question, the use

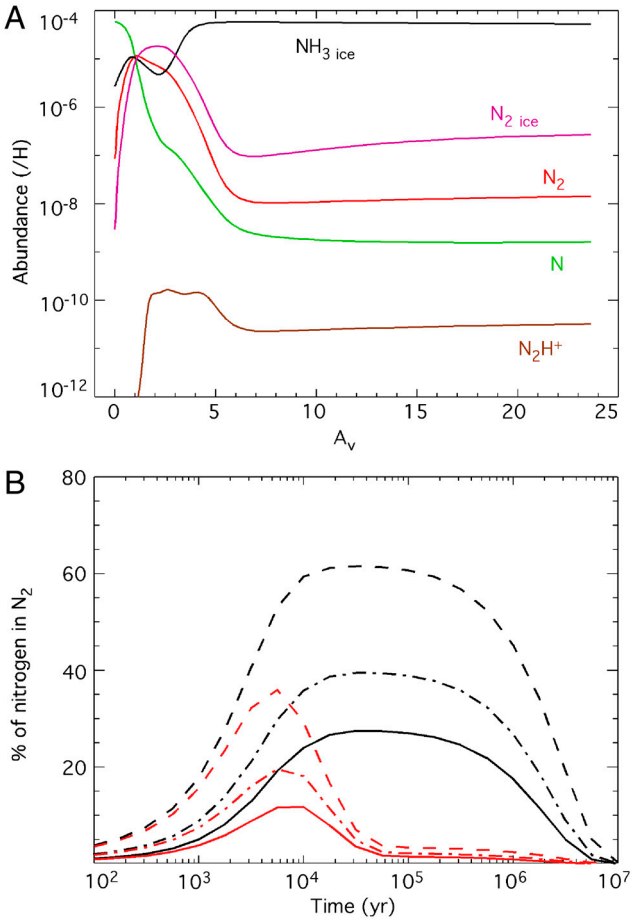


**Fig. 5.** Model results for the B68 prestellar core using a C/O elemental ratio of 1.2. (*A*) Gas phase abundances of N, $N_2$, $N_2H^+$ and ice abundances of $N_2$ and $NH_3(/n_H)$ as a function of visual extinction for model (*c*) at an age of $5 \times 10^6$ yr. (*B*) Percentage of elemental nitrogen in the form of $N_2$ (in the gas-phase and on interstellar ices) as a function of time. Red lines indicate gas-phase $N_2$, black lines indicate total (gas + ice) $N_2$ with three different networks: dashed lines, model (*a*) OSU database; dashed-dotted lines, model (*b*) KIDA values (17); solid lines, model (*c*) KIDA with updates for reactions **1**, **2**, and **4**.

of lower rate constants for reactions **1**, **2**, and **4** while considering depletion onto grain surfaces indicates that the ultimate reservoir of nitrogen in interstellar environments is unlikely to be $N_2$ either in the gas-phase or on the grain surfaces. This result has potential consequences for our view of the development of the early Earth, which probably possessed a neutral atmosphere consisting of mostly $CO_2$ and $N_2$. As considerable energy is required to break N out of $N_2$, other nitrogen bearing molecules such as ammonia in interplanetary dust from the primitive nebula have been proposed as possible sources of fixed nitrogen easily usable by the first forms of life on Earth (34).

## Materials and Methods

**Experimental.** Experiments were performed using a miniaturized continuous supersonic flow reactor modified from the original apparatus designed by Rowe et al. (11) The main features of the present system have been previously described (7). Briefly, four Laval nozzles were used to perform kinetic measurements at specified temperatures of 56 K, 87 K, 152 K, and 169 K. Measurements at 296 K were performed in the reactor by removing the nozzle and by significantly reducing the flow velocity to eliminate pressure gradients in the observation region. Ground-state atomic nitrogen was generated upstream of the Laval nozzle by the microwave discharge technique. A Vidal type microwave discharge cavity (35) operating at 2.45 GHz and up to 200 W was mounted on one of the quartz inlet tubes entering the Laval nozzle reservoir. In this way, excess concentrations of ground state atomic nitrogen estimated to be as high as $3.3 \times 10^{14}$ cm$^{-3}$ could be produced. An earlier study (7) showed that atomic nitrogen in excited states $N(^2P^0)$ and $N(^2D^0)$ was negligible in the supersonic flow under similar conditions. The high discharge power used to produce excess atomic nitrogen also resulted in elevated gas temperatures within the nozzle reservoir. Moreover, the reservoir temperature was also found to vary as a function of the molecular nitrogen flow through the discharge during some experiments. As a result, for a specified nozzle, the discharge power was varied for different molecular nitrogen flows to maintain a constant reservoir temperature, as verified by a type K thermocouple inserted into the reservoir prior to the experiments. At the same time, the supersonic flow was characterized through the measurement of the impact pressure using a Pitot tube to verify that the microwave discharge did not perturb the downstream flow. The measured reservoir temperatures and impact and stagnation pressures were subsequently employed in the flow calculations.

OH radicals in the $X^2\Pi_i$ state were generated by the in situ pulsed photodissociation of $H_2O_2$ using the unfocused output of a 10 Hz frequency quadrupled Nd:YAG laser at 266 nm with approximately 22 mJ of pulse energy. $H_2O_2$ was introduced into the flow by bubbling a small flow of the carrier gas through a 50% weight mixture of $H_2O_2/H_2O$. An upper limit of $3.6 \times 10^{13}$ cm$^{-3}$ was estimated for the gas phase concentration of $H_2O_2$ in the supersonic flows and $5.0 \times 10^{13}$ cm$^{-3}$ at 296 K from its saturated vapor pressure, providing OH concentrations lower than $4.3 \times 10^{11}$ cm$^{-3}$ in the supersonic flows and $6.0 \times 10^{11}$ cm$^{-3}$ at 296 K from calculations of the photodissociation efficiency of $H_2O_2$. Simultaneously, CN radicals in the $X^2\Sigma^+$ state were generated by the 266 nm photolysis of ICN molecules entrained in the flow by passing a small flow of carrier gas over a sample of solid ICN held in a separate container. An upper limit of $2.1 \times 10^{12}$ cm$^{-3}$ was estimated for the gas phase concentration of ICN in the supersonic flows and $5.2 \times 10^{12}$ cm$^{-3}$ at 296 K from its saturated vapor pressure. CN concentrations in the supersonic flow and at 296 K were estimated to be $8.5 \times 10^{10}$ and $2.0 \times 10^{11}$ cm$^{-3}$, respectively. From the estimated minor reagent densities, reaction between CN and OH should not occur to any great extent in the flow. Nevertheless, test experiments were performed that showed that OH decays recorded in the absence of CN yielded identical first-order rate constants to those obtained when CN was present in the flow, confirming this hypothesis.

The probe laser system for the detection of OH radicals by laser-induced fluorescence (LIF) has been described previously (36). CN radicals were followed by LIF via the R-branch lines of the (1, 0) $B^2\Sigma^+ \leftarrow X^2\Sigma^+$ band. For this purpose, the third harmonic 355 nm radiation of a pulsed single longitudinal mode Nd:YAG laser was used to pump an OPO system to produce tuneable radiation around 538 nm. This radiation was sum frequency mixed with the residual fundamental radiation of the same Nd:YAG laser at 1064 nm in a BBO crystal to produce tuneable radiation around 357.55 nm. CN radicals were observed via the $B^2\Sigma^+ \rightarrow X^2\Sigma^+$ (1, 1) band using a second UV sensitive PMT coupled with a 10 nm FWHM interference filter centered on 390 nm and a second boxcar integrator. Both probe lasers were coaligned and counterpropagated with respect to the photolysis laser in the reactor.

LIF signals from the reactant OH and CN radicals were recorded simultaneously. For a given atomic nitrogen concentration, 30 data points were accumulated at each time interval with both temporal profiles consisting of a minimum of 46 time intervals. This procedure was repeated for each atomic nitrogen concentration for a minimum of nine different atomic nitrogen concentrations. As CN and OH signals were potentially non-zero in the absence of the photolysis laser (due to the possible upstream production of CN and OH radicals by the microwave discharge), several time points were recorded by firing the probe lasers before the photolysis laser. The LIF intensities were measured at a fixed distance from the Laval nozzle; the chosen distance corresponded to the maximum displacement from the nozzle for optimal flow conditions to be still valid, thus allowing us to exploit the fluorescence signals over as large a period as possible. Simple exponential fits to the OH and CN temporal profiles yielded the pseudo-first order rates for reactions **1** and **4**, $k'_1$ and $k'_4$ respectively. Nevertheless, it should be noted that as $k'_1$ and $k'_4$ contain the additional loss terms $k_{L,OH}$ and $k_{L,CN}$—the losses of OH and CN, respectively, by diffusion from the zone illuminated by the probe laser (which is smaller than the cross sectional area of the supersonic flow) or through secondary reactions—we do not expect the fits to pass through the origin. In the absence of atomic nitrogen, this y-axis intercept value is equal to $k_{L,CN}$-m $k_{L,OH}$ where $m$ is the slope. As a result of the increasing value of $m$, the intercept value is expected to become more negative at higher temperatures.

**Chemical Model.** To simulate interstellar chemistry, the Nautilus gas-grain model was used, which allows us to numerically solve a series of coupled differential equations. This model computes the species abundances as a function of time for a given set of physical parameters, starting from an

initial chemical composition. A chemical network of 4,394 gas-phase reactions and 1,748 grain-surface and gas-grain reactions was used, with values recommended by the KIDA database with the exceptions being reactions **1**, **2**, and **4**. A more detailed description of the model itself can be found in Semenov et al. (37). This model has been used to study the chemistry in several types of environments such as dark molecular clouds (19) and protoplanetary disks (38, 39). In our model, ammonia is formed on grains by the successive hydrogenation of nitrogen atoms that stick on grain surfaces through the Langmuir-Hinshelwood mechanism (40).

For the prestellar core models, we have taken the example of Barnard 68, whose physical structure has been well studied (26, 41). The density structure is well reproduced by a Bonnor Ebert sphere with a central density of $5 \times 10^5$ cm$^{-3}$ (26). We have used Nautilus in a 1D geometry with this density structure and assumed a constant temperature of 10 K, following Maret et al. (6). The visual extinction is computed as a function of the radius to the centre of the core by integrating the $H_2$ column density. The penetration of the external UV photons (using the standard UV interstellar field) is computed as a function of this visual extinction. The chemical composition of the core is then computed as a function of time assuming that the physical structure does not change during this time. As for dense clouds, we have assumed that species are initially in atomic form, except for $H_2$.

**ACKNOWLEDGMENTS.** The experimental work was supported by the Agence Nationale de la Recherche (ANR-JC08_311018), the Conseil Régional d'Aquitaine (20091102002), the European Union (PERG03-GA-2008-230805) and the Centre National de la Recherche Scientifique (CNRS) interdisciplinary program Environnements Planétaires et Origines de la Vie. The experimental and modeling work were both supported by the Institut National des Sciences de l'Univers-CNRS national program Physique et Chimie du Milieu Interstellaire and the Observatoire Aquitain des Sciences de l'Univers.

1. Knauth DC, Andersson B-G, McCandliss SR, Moos HW (2004) The interstellar $N_2$ abundance towards HD 124314 from far-ultraviolet observations. *Nature* 429:636–638.
2. Viala YP (1986) Chemical equilibrium from diffuse to dense interstellar clouds. I. Galactic molecular clouds. *Astron Astrophys Suppl Ser* 64:391–437.
3. Bergin EA, Langer WD (1997) Chemical evolution in preprotostellar and protostellar cores. *Astrophys J* 486:316–328.
4. Herbst E, Klemperer W (1973) The formation and depletion of molecules in dense interstellar clouds. *Astrophys J* 185:505–533.
5. Womack M, Ziurys LM, Wyckoff S (1992) Estimates of $N_2$ abundances in dense molecular clouds. *Astrophys J* 393:188–192.
6. Maret S, Bergin EA, Lada CJ (2006) A low fraction of nitrogen in molecular form in a dark cloud. *Nature* 442:425–427.
7. Daranlot J, et al. (2011) Revealing atom-radical reactivity at low temperature through the N + OH reaction. *Science* 334:1538–1541.
8. Bergeat A, et al. (2009) A low temperature investigation of the $N(^4S^0) + NO$ reaction. *Phys Chem Chem Phys* 11:8149–8155.
9. Jorfi M, Honvault P (2009) State-to-state quantum reactive scattering calculations and rate constant for nitrogen atoms in collision with NO radicals at low temperatures. *J Phys Chem A* 113:10648–10651.
10. Gamallo P, Martínez R, Sayós R, González M (2010) Quasiclassical dynamics and kinetics of the $N + NO \rightarrow N_2 + O$, $NO + N$ atmospheric reactions. *J Chem Phys* 132:144304.
11. Rowe BR, Dupeyrat G, Marquette JB, Gaucherel P (1984) Study of the reactions $N_2^+ + 2N_2 \rightarrow N_4^+ + N_2$ and $O_2^+ + 2O_2 \rightarrow O_4^+ + O_2$ from 20 to 160 K by the CRESU technique. *J Chem Phys* 80:4915–4921.
12. Sims IR, et al. (1992) Ultra-low temperature kinetics of neutral-neutral reactions: The reaction $CN + O_2$ down to 26 K. *J Chem Phys* 97:8798–8800.
13. Berteloite C, et al. (2010) Kinetics and dynamics of the $S(^1D_2) + H_2 \rightarrow SH + H$ reaction at very low temperatures and collision energies. *Phys Rev Lett* 105:203201.
14. Carty D, Goddard A, Köhler SPK, Sims IR, Smith IWM (2006) Kinetics of the radical-radical reaction, $O(^3P_J) + OH(X^2\Pi_\Omega) \rightarrow O_2 + H$, at temperatures down to 39 K. *J Phys Chem A* 110:3101–3109.
15. Whyte AR, Phillips LF (1983) Rate of reaction of N with CN ($v = 0$, 1). *Chem Phys Lett* 98:590–593.
16. Atakan B, Kocis D, Wolfrum J, Nelson P (1992) Direct investigations of the kinetics of the reactions of CN radicals with N atoms and $^3CH_2$ radicals with NO. *Symp (Int) Combust [Proc]* 691–699.
17. Wakelam V, et al. (2012) A KInetic Database for Astrochemistry (KIDA),. *Astrophys J Suppl Ser* 199:21.
18. Woodall J, Agúndez M, Markwick-Kemper AJ, Millar TJ (2012) The UMIST database for astrochemistry 2006. *Astron Astrophys* 466:1197–1204.
19. Hincelin U, et al. (2011) Oxygen depletion in dense molecular clouds: A clue to low $O_2$ abundance? *Astron Astrophys* 530:A61.
20. Jenkins EB (2009) A unified representation of gas-phase element depletions in the interstellar medium. *Astrophys J* 700:1299–1348.
21. Whittet DCB (2010) Oxygen depletion in the interstellar medium: Implications for grain models and the distribution of elemental oxygen. *Astrophys J* 710:1009–1016.
22. Pratap P, et al. (1997) A study of the physics and chemistry of TMC-1. *Astrophys J* 486:862–885.
23. Akyilmaz M, Flower DR, Hily-Blant P, Pineau des Forêts G, Walmsley M (2007) The depletion of NO in pre-protostellar cores. *Astron Astrophys* 462:221–230.
24. Hily-Blant P, Walmsley M, Pineau des Forêts G, Flower D (2010) Nitrogen chemistry and depletion in starless cores. *Astron Astrophys* 513:A41.
25. Rodgers SD, Charnley SB (2008) Nitrogen isotopic fractionation of interstellar nitriles. *Astrophys J* 689:1448–1455.
26. Alves JF, Lada CJ, Lada EA (2001) Internal structure of a cold dark molecular cloud inferred from the extinction of background starlight. *Nature* 409:159–161.
27. Sandford SA, Bernstein MP, Allamandola LJ, Goorvitch D (2001) Teixeira TCVS The abundances of solid $N_2$ and gaseous $CO_2$ in interstellar dense molecular clouds. *Astrophys J* 548:836–851.
28. Cesaroni R, Churchwell E, Hofner P, Walmsley CM, Kurtz S (1994) Hot ammonia towards compact HII regions. *Astron Astrophys* 288:903–920.
29. Bottinelli S, et al. (2010) The c2d Spitzer spectroscopic survey of ices around low-mass young stellar objects. IV $NH_3$ and $CH_3OH$. *Astrophys J* 718:1100–1117.
30. Chiar JE, et al. (2011) Ices in the quiescent IC 5146 dense cloud. *Astrophys J* 731:9.
31. Gibb EL, et al. (2000) An inventory of interstellar ices toward the embedded protostar W33A. *Astrophys J* 536:347–356.
32. Wakelam V, et al. (2010) Reaction networks for interstellar chemical modelling: Improvements and challenges. *Space Sci Rev* 156:13–72.
33. Bockelée-Morvan D, Crovisier J, Mumma MJ, Weaver HA (2004) *The Composition of Cometary Volatilesin* Comets II, eds MC Festou, HU Keller, and HA Weaver (University of Arizona Press, Tucson), pp 391–423.
34. Chyba C, Sagan C (1992) Endogeneous production, exogeneous delivery and impact-shock synthesis of organic molecules: An inventory for the origin of life. *Nature* 355:125–132.
35. Vidal B, Dupret C (1976) Experimental study of new microwave cavities to produce plasmas and free radicals to initiate chemiluminescences. *J Phys E: Sci Instrum* 9:998–1002.
36. Daranlot J, et al. (2010) Gas-phase kinetics of hydroxyl radical reactions with alkenes: Experiment and theory. *Chem Phys Chem* 11:4002–4010.
37. Semenov D, et al. (2010) Chemistry in disks. IV. Benchmarking gas-grain chemical models with surface reactions. *Astron Astrophys*, p:A42.
38. Hersant F, Wakelam V, Dutrey A, Guilloteau S, Herbst E (2009) Cold CO in circumstellar disks: On the effects of photodesorption and vertical mixing. *Astron Astrophys* 493: L49–L52.
39. Dutrey A, et al. (2011) Sulfur-bearing molecules in the protoplanetary disks surrounding LkCa15, MWC480, DM Tauri, and GO Tauri. *Astron Astrophys* 535:A104.
40. Hasegawa TI, Herbst E, Leung CM (1992) Models of gas-grain chemistry in dense interstellar clouds with complex organic molecules. *Astrophys J Suppl* 82:167–195.
41. Bergin EA, et al. (2006) The thermal structure of gas in prestellar cores: A case study of Barnard 68. *Astrophys J* 645:369–380.